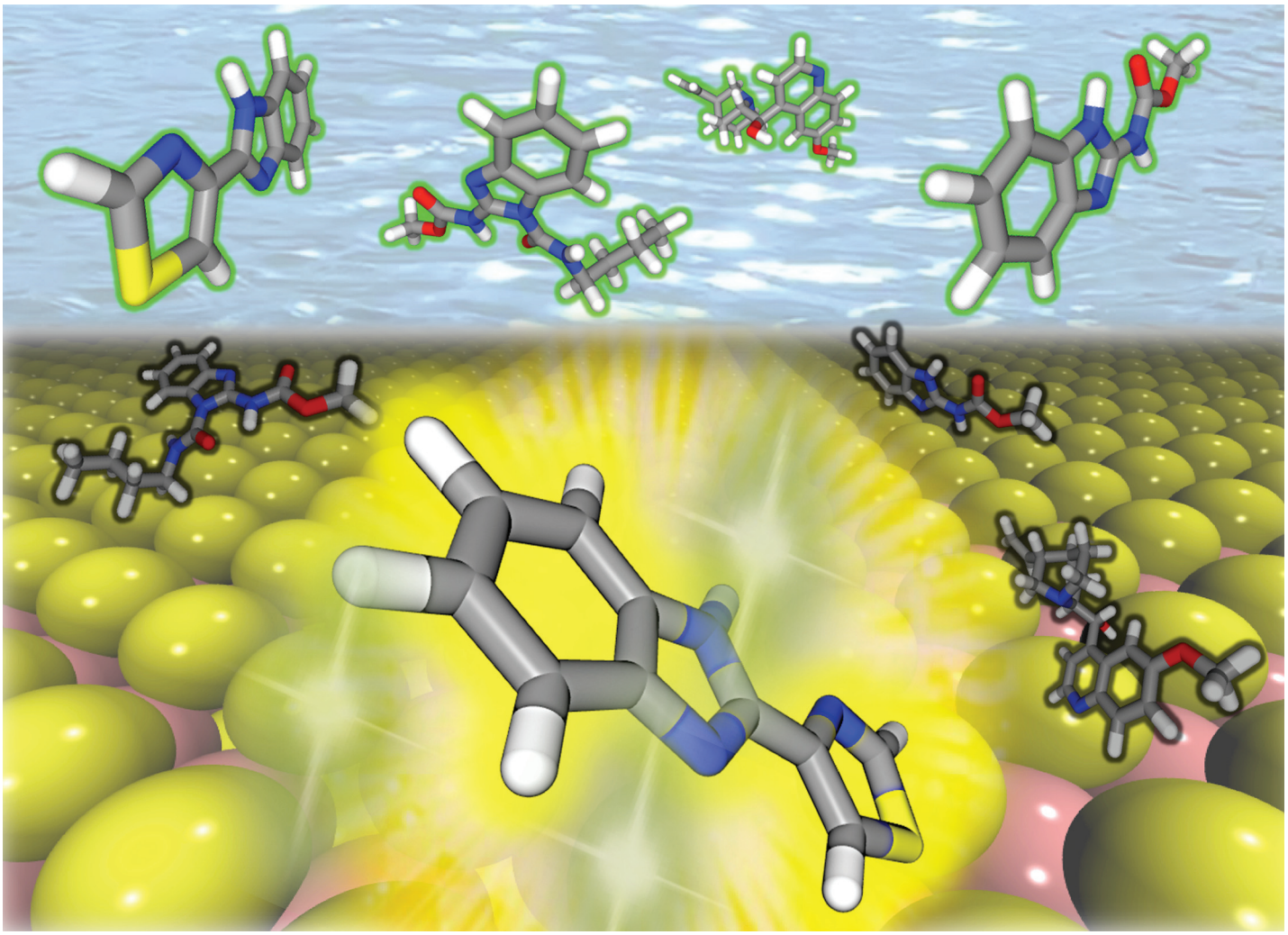

Showcasing research from the Institute of Materials Science (CSIC) and Analytical Chemistry and Instrumental Analysis Department (UAM), Madrid, Spain.

Fluorescence enhancement of fungicide thiabendazole by van der Waals interaction with transition metal dichalcogenide nanosheets for highly specific sensors

DFT calculations allow rationalization of the surprising fluorescence enhancement that thiabendazole exhibits because of its interaction with transition metal dichalcogenides (TMDs). This effect, non-observed for other fungicides nor when thiabendazole interacts with other nanomaterials, is related to a small molecular distortion after the non-covalent adsorption of thiabendazole on TMDs, inhibiting the intramolecular rotation between the benzimidazole and thiazole groups. Based on this effect, a sensitive and selective method for thiabendazole analysis in river water is developed.

As featured in:

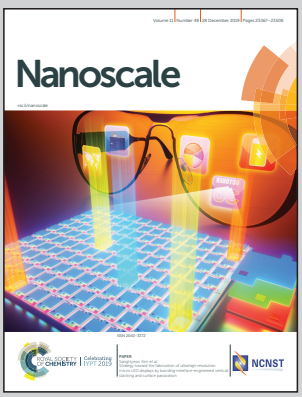

See Carmen Quintana *et al.*, *Nanoscale*, 2019, **11**, 23156.

ROYAL SOCIETY OF CHEMISTRY | Celebrating IYPT 2019

rsc.li/nanoscale

Registered charity number: 207890

Nanoscale

PAPER

View Article Online
View Journal | View Issue

Cite this: *Nanoscale*, 2019, **11**, 23156

Fluorescence enhancement of fungicide thiabendazole by van der Waals interaction with transition metal dichalcogenide nanosheets for highly specific sensors†

Elías Blanco, [a] José I. Martínez, [b] Ana María Parra-Alfambra, [a] María Dolores Petit-Domínguez, [a] María del Pozo, [a] José A. Martín-Gago, [b] Elena Casero [a] and Carmen Quintana *[a]

Many molecules quench their fluorescence upon adsorption on surfaces. Herein we show that the interaction of thiabendazole, a widespread used fungicide of the benzimidazole family, with nanosheets of transition metal dichalcogenides, particularly of WS_2, leads to a significant increase, more than a factor of 5, of the fluorescence yield. This surprising effect is rationalized by DFT calculations and found to be related to the inhibition of the intramolecular rotation between the benzimidazole and thiazole groups due to a bonding rigidization upon interaction with the MoS_2 surface. This non-covalent adsorption leads to a redistribution of the molecular LUMO that blocks the non-radiative energy dissipation channel. This unusual behaviour does not operate either for other molecules of the same benzimidazole family or for other 2D materials (graphene or graphene oxide). Moreover, we found that a linear dependence of the emission with the concentration of thiabendazole in solution, which combined with the specificity of the process, allows the development of a highly sensitive and selective method towards thiabendazole determination that can be applied to real river water samples. An excellent detection limit of 2.7 nM, comparable to the best performing reported methods, is obtained with very good accuracy ($E_r \leq 6.1\%$) and reproducibility (RSD $\leq 4.1\%$) in the concentration range assayed.

Received 1st April 2019,
Accepted 22nd August 2019

DOI: 10.1039/c9nr02794g

rsc.li/nanoscale

Introduction

Transition metal dichalcogenides (TMDs) have been proposed as new kinds of 2D materials to be used in a large number of applications, such as optoelectronics devices, energy harvesting materials, or advanced batteries.[1–4] However, although there are some examples related to the use of TMDs for the development of chemical sensors, the benefits derived from their use are still not profusely explored. Recently, MoS_2 nanosheets have been proved to exhibit a synergistic effect when combined with other nanomaterials such as graphene,[5] gold nanoparticles[6] and diamond nanoparticles,[7] allowing the design of electrochemical sensors and biosensors with improved analytical properties.[8] Moreover, the interaction in solution of these nanomaterials with different compounds has been employed to develop new analytical methodologies, as this interaction leads to changes in light emission properties.[9,10] Usually, the interaction of a fluorescent molecular compound with the surface of nanomaterials leads to a quenching of its light emission which has been extensively used for sensing specific (bio)molecules.[10–13] Similar strategies based on the fluorescence changes of dye–TMD conjugates have been successively applied for the detection of biomarkers for different cellular processes even for cancer diagnostics.[14–16] However, we show here an unprecedented example of enhancement (>5×) of the fluorescence yield of thiabendazole (TBZ), a widespread fungicide molecule of the benzimidazole family, after non-covalent interactions with the surface of different TMDs.

Herein we have explored the interaction between different fungicides of the benzimidazole family, such as carbendazim

[a]*Departamento de Química Analítica y Análisis Instrumental, Facultad de Ciencias, Francisco Tomás y Valiente, N°7, Campus de Excelencia de la Universidad Autónoma de Madrid, 28049 Madrid, Spain. E-mail: carmen.quintana@uam.es*
[b]*Materials Science Factory, Institute of Materials Science of Madrid (ICMM-CSIC), Sor Juana Inés de la Cruz, N°3, 28049 Madrid, Spain*

†Electronic supplementary information (ESI) available: Influence of the nanomaterials and solvent amount employed to TMDs exfoliation on the fungicide fluorescence, description of the different DFT-optimized (CBZ/TBZ)/MoS_2, (CBZ/TBZ)/Gr, and (CBZ/TBZ)/GOx interfacial configurations, density of electronic states for the free CBZ and TBZ molecules, and for the optimized (CBZ/TBZ)/MoS_2, (CBZ/TBZ)/Gr, and (CBZ/TBZ)/GOx interfacial configurations, and different methods for determination of TBZ and detection limits. See DOI: 10.1039/c9nr02794g

(CBZ), benomyl (BN), and TBZ, and 2D nanoplatforms of different TMDs produced by solvent-assisted exfoliation (MoS_2 and WS_2) and graphene oxide (GOx). Our results show that in all the fungicides assayed, the fluorescence is quenched but in TBZ it is largely enhanced (see Scheme 1). Interestingly, the interaction of TBZ with GOx nanosheets also importantly reduces its fluorescence. We have rationalized the process by density functional theory (DFT) calculations which reveal that the enhancement is produced by an adsorption geometry that induces a bending of the molecular structure leading to efficient electron transfer from the HOMO to the LUMO orbital, which is redistributed into the benzimidazole group. This curvature-induced effect is specific for this molecule of the family on the surface of TMDs.

Aggregation-Induced Emission (AIE) has been depicted as a photophysical phenomenon leading to fluorescence enhancement by molecular aggregation in many systems[17,18] (and references therein). In this work, a similar mechanism is outlined by DFT on a surface-mediated AIE due to the rigidization of the C–C bonds that inhibits the intramolecular rotation between the benzimidazole and thiazole groups upon non-covalent adsorption on TMD surfaces.

We have used the specificity and robustness of the process to design a fluorescence method to quantify the TBZ concentration in real samples. TBZ is a general biocide with fungicide and nematicide activities that, as the rest of the benzimidazole fungicides, presents fluorescence properties.[19–21] In humans and livestock, TBZ has shown activity against the parasitic worms helminths, although a high dosage of TBZ in rats can be carcinogenic and the chronic exposure to benzimidazole residues has been linked with embryotoxicity, teratogenicity and anemia.[19,20] In agriculture, benzimidazoles are used for pre- and post-harvest treatments to avoid various fungi and can be applied directly to the soil or sprayed over the fields so these compounds can migrate to groundwater systems. Because they can be used for many applications, their use is widespread and they can be found in wastewaters from the agricultural industry and urban areas.[19,21,22] Many different methods for the detection of TBZ have been proposed, including surface-enhanced Raman spectroscopy (SERS) (allowing the analysis in solid samples),[21] electrochemical[23] or different luminescence techniques.[22] Nevertheless, most of the methods proposed require the use of sophisticated equipment such as high performance liquid chromatography.[19,20] We show hereafter that a sensor based on our findings exhibits not only one of the lower detection limits reported (2.7 nM) but also high selectivity towards other compounds of the same family.

Results and discussion

Fluorescence enhancement of TBZ

We have isolated 2D layers (nanosheets) of different TMDs by chemical exfoliation in solution. Fig. 1A shows the fluorescence emission spectra recorded from TBZ aqueous solution in the absence and in the presence of different nanomaterials. In the absence of the 2D nanomaterial (spectrum a), TBZ solution presents a fluorescence maximum value at

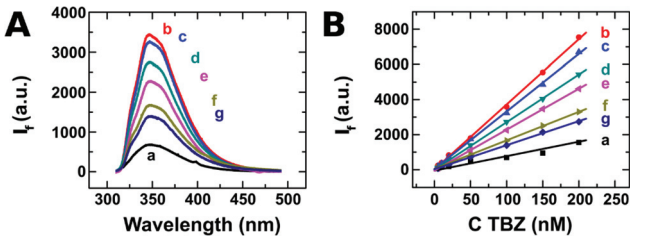

Fig. 1 (A) Fluorescence spectra of 100 nM TBZ (final concentration) without a nanomaterial (curve a) and with suspension of different 2D TMDs in different solvents (curves b–g). TBZ + WS_2 90 nm EtOH/H_2O (curve b), TBZ + MoS_2 90 nm EtOH/H_2O (curve c), TBZ + MoS_2 2 μm EtOH/H_2O (curve d), TBZ + WS_2 90 nm NMP (curve e), TBZ + MoS_2 90 nm NMP (curve f) and TBZ + MoS_2 2 μm NMP (curve g). (B) Influence of TBZ initial concentration on the fluorescence yield measured at λ_{em} = 350 nm; λ_{exc} = 294 nm. TMDs: 200 μL to 5.00 mL final volume.

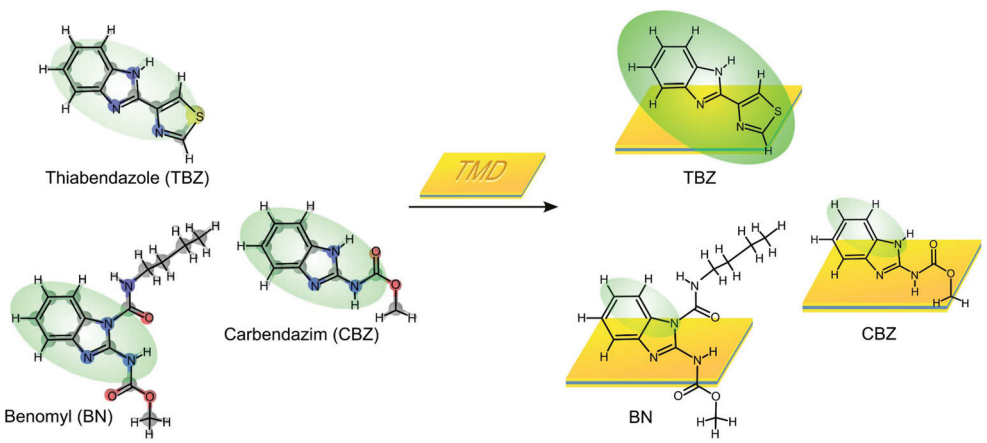

Scheme 1 Illustration of the fluorescence phenomena of different benzimidazole pesticides after interaction with TMDs.

350 nm. Surprisingly, this initial fluorescence signal increases to a great extent in the presence of all the TMD materials assayed (curves b–g). The highest increase is observed for the case of WS_2 exfoliated in EtOH/H_2O (curve b), which exhibits a 5-fold fluorescence increment with respect to the signal without the nanomaterial. It should be noted that neither the nanomaterials nor equivalent amounts of the solvents employed for TMD exfoliation produced a fluorescence signal at 350 nm (see Fig. S1 in the ESI†). Other suspensions produced lower increments in the TBZ initial signal, but even in the worst example, MoS_2 2 μm NMP (curve g), a 2-fold increase with respect to the case without the nanomaterial, is observed. We have confirmed this behaviour by performing the same experiment with different initial TBZ concentrations (between 5 and 200 nM) and keeping constant the amount of TMDs. These results are shown in Fig. 1B, where the increase of TBZ concentration leads to a linear increase in the recorded emission with correlation coefficients higher than 0.997 for every 2D nanomaterial. In this concentration range, the highest sensitivity in detecting TBZ is achieved with WS_2 exfoliated with EtOH/H_2O with a slope of 37.1 nM^{-1} (Fig. 1B, curve b). In contrast, if the calibration procedure is performed without TMD, 4.4 fold lower sensitivity (8.4 nM^{-1}) is registered (Fig. 1B, curve a).

These results are quite surprising since most of the studies reported in the literature about the interaction of 2D materials with different compounds describe a decrease in the fluorescence emission of a target molecule when exposed to nanomaterials as a consequence of the quenching induced by the interaction of the molecule with the surface. As an example, fluorescent carbon dots and ss-DNA labelled with the fluorescent probe showed quenching when exposed to 2D nanomaterials such as MoS_2 and Ta_2NiS_5.[10,13] Moreover, it was found that the forces involved in the interaction with TMDs are van der Waals forces, whilst GOx uses a hydrogen bond and π–π stacking to interact.[24]

In view of these results, we selected three different molecules owing to the same fluorescent benzimidazole group, to be evaluated in the presence of MoS_2: two fungicides similar to TBZ in structure and emission properties (CBZ and BN), and quinine (Q) as the fluorescent probe with a very well-known fluorescence behaviour (see Scheme S1 in the ESI†). Fig. 2(A–C) shows the emission spectra recorded from solutions of each compound in the absence (spectra a) and in the presence (spectra b) of the nanomaterial. In all cases, the presence of TMDs led to a clear decrease in the fluorescence yield measured at their maximum emission wavelength. For instance, the fluorescence intensities of CBZ and BN (Fig. 2A and B) were quenched 73% and 65%, respectively. As shown in Fig. 2C, similar results were obtained when the experiment was performed with Q, which exhibited a noticeable decrease in its fluorescence intensity in the presence of MoS_2. This indicates that fluorescence measurements in the presence of TMDs can be used as an efficient sensing method of TBZ, with low interference from other similar molecules of the same family, which importantly decrease the fluorescence efficiency.

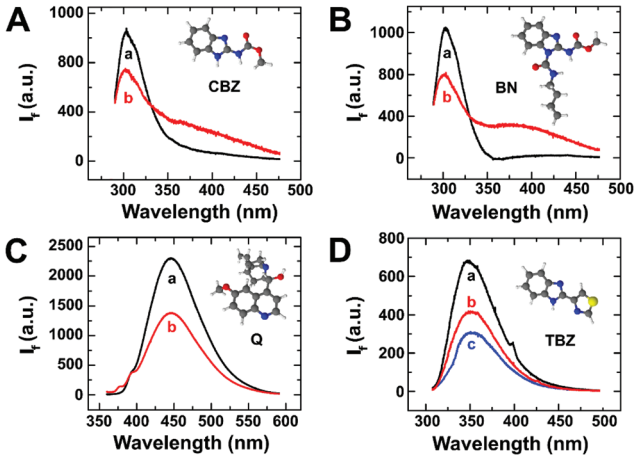

Fig. 2 Fluorescence emission spectra of (A) 2.50 μM CBZ, (B) 2.00 μM BN and (C) 0.500 μM Q in the absence (curve a) and in the presence (curve b) of MoS_2 90 nm. λ_{exc} = 280 nm (CBZ and BN), 445 nm (Q). (D) 100 nM TBZ before (curve a) and after (curve b) the addition of GOx and (curve c) addition of MnO_2. λ_{exc} = 294 nm.

Moreover, we wondered whether this effect is exclusive of TMDs or it can be found on other 2D materials, such as GOx or MnO_2. Fig. 2D shows a decrease of the TBZ fluorescence emission of about 40% and 60% when exposed to GOx and MnO_2, respectively, similar to that reported in the literature.[24]

Theoretical calculations and rationalization of the process

In an attempt to rationalize the mechanism leading to the on-surface fluorescence enhancement, we have theoretically analysed the case of two representative molecules, TBZ and CBZ, for which we have simulated their structural, electronic and excitation properties in both their free forms, as well as adsorbed on the surface of different nanomaterials (MoS_2, graphene and graphene oxide single layers, with different concentrations of defects) by means of a large battery of first-principles static/time-dependent DFT-based (TDDFT), and single-excitation calculations (see ESI, sections S2 and S3†). It is important to remark that a direct comparison between the experimental fluorescence (Fig. 1) and the computed photoexcitation spectra is not truthful, since we are missing the relaxation of the excited states and the possible emerging excitonic effects. Nevertheless, the calculation of photoexcitation can provide very valuable information that can be related to the emission spectra, such as the relative intensity (and efficiency) of the transitions, wavelength shifts from one system to another, and the origin of the most important transitions (initial and final electronic states), among others. This strategy has been recently followed to successfully explain very interesting experimental emission effects.[25–27]

The top panel of Fig. 3 shows the optimized geometries and the most stable configurations for CBZ (Fig. 3A) and TBZ (Fig. 3B) molecules, both free and adsorbed on a single layer of MoS_2 (for each system the figure shows those configurations lying within a total energy range of <0.2 eV). Within all the

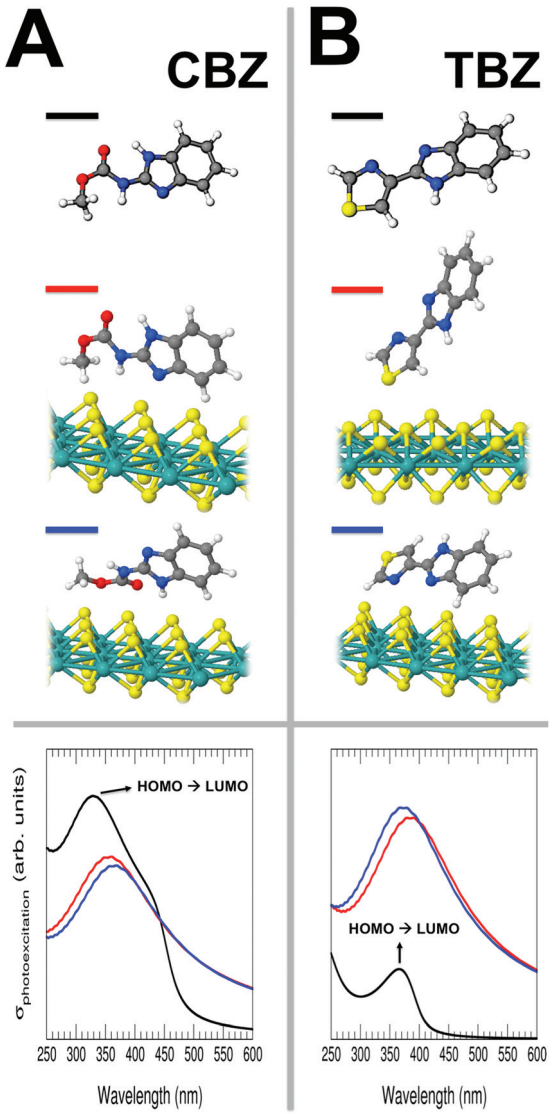

Fig. 3 Pictorial views of the DFT-based optimized free and interfacial systems and computed TDDFT photoexcitation spectra for: (A) free CBZ molecule (black line) and the two most stable CBZ/MoS_2 interfacial configurations (red and blue lines); and (B) free TBZ molecule (black line) and the two most stable TBZ/MoS_2 interfacial configurations (red and blue lines).

interfacial systems analysed, the character of the molecule/substrate interaction is mainly driven by electrostatic and van der Waals forces, exhibiting an almost negligible chemical interaction. Nonetheless, in most cases, this interaction is strong enough to anchor the molecules to the surface, even to significantly modify the gas-phase molecular geometries. We have checked that the presence of a large number of S-vacancies in the substrate does not importantly alter these results (see Fig. S4 of the ESI†).

Starting with the CBZ/MoS_2 interface (Fig. 3A), the preferential molecular adsorption configurations show, in one case, the molecule tending to maximize the interaction with the substrate *via* the non-hydrogenated N atom of the molecular pentagon and the terminating –CH_3 group of the ester (second geometry, red line in Fig. 3A), whilst in the other configuration (third geometry, blue line in Fig. 3A), the molecule interacts with the substrate *via* the –$COOCH_3$ ester group, leaving the rest of the molecule slightly twisted away. These two configurations yield molecular binding energies of 0.95 and 1.10 eV, respectively and therefore, both of them are plausible.

For the TBZ/MoS_2 case (Fig. 3B), one of the preferential molecular adsorption configurations (second geometry, red line in Fig. 3B) shows the molecule interacting with the substrate *via* its terminating S-atom (at an adsorption perpendicular distance w.r.t. the average topmost S-plane of around 2.2 Å), yielding a binding energy of around 1.15 eV. This particular substrate/adsorbate interaction induces a net molecular distortion characterized by a bending after the adsorption of around 0.4 Å (see ESI, top panel of Fig. S3B†), which will have a clear reflection on its electronic and excitation properties, as explained below. In the other configuration (third geometry, blue line in Fig. 3B), the molecule again tends to maximize the interaction with the substrate *via* the non-hydrogenated N atom of the molecular pentagon with a very close binding energy value w.r.t. the previous configuration, 1.18 eV, again exhibiting a slightly bent molecular geometry of around 0.3 Å once deposited on MoS_2 (see ESI, bottom panel of Fig. S3B†). The geometrical distortions induced in the TBZ molecule after adsorption on MoS_2 provide a clue about the high flexibility of the C–C bond connecting its thiazole and benzimidazole counterparts, which is directly linked to its fluorescence properties. As in the case of CBZ, the small differences in the adsorption energy suggest that both configurations are plausible. It is important to note that there is no chemical bonding between the S atoms from the molecule and from the surface, but the interaction remains electrostatic.

The bottom panel of Fig. 3A and B shows the computed TDDFT photoexcitation spectra of the free CBZ and TBZ molecules (black lines) and the two most stable configurations (red and blue lines) for each CBZ/MoS_2 and TBZ/MoS_2 interfaces. At this point, it is important to remark again that the calculation of the photoexcitation provides exclusively qualitative information about the energy distribution and more quantitative with respect to the relative intensity (and efficiency) of the transitions, as the origin of the most important transitions (initial and final electronic states) is well captured by the code.

Interestingly, the photoexcitation spectra in Fig. 3 show a correlating result with the experimental observations. The spectrum computed for the free CBZ exhibits a pronounced peak at around 330 nm. A configuration interaction single-excitation (CIS) calculation has permitted us to elucidate that the origin of this excitation is a transition between the molecular HOMO and LUMO states with a weight of 73% (the resting contribution comes mainly from the HOMO−2 → LUMO transition). The computed photoexcitation spectra for the two most stable CBZ/MoS_2 interfacial configurations show a similar profile between them, but a global decrease of the photoexcitation intensity after interaction with MoS_2 due to the loss of efficiency of this particular optical transition.

Besides, a slight red-shift up to wavelengths of around 350 nm is observed when the molecule is adsorbed on the substrate together with an enlargement of the queue that is reproduced in the experiments as shown in Fig. 2A (curve b).

In contrast, for the free TBZ molecule, the intensity of the most pronounced peak in the photoexcitation spectrum (at around 365 nm) is much lower than that for the most stable interfacial configurations where the TBZ molecule is adsorbed on the MoS_2 substrate, exhibiting an increase of the photoexcitation intensity by around ×4. Once again, the origin of this excitation in the gas-phase molecule is a transition between the molecular HOMO and LUMO states with a weight of 78% (the rest of the contribution comes also mainly from the HOMO−2 → LUMO transition). This dramatic increase in the photoexcitation signal (directly linked with the gain in the efficiency in the optical transition) has its reflection in the experimental observation of the fluorescence of this molecule when it is deposited on the substrate. Again, a slight red-shift is also observed in this case when the molecule is adsorbed on the substrate. It is interesting to mention that the different wavelengths for the most important peak in both molecules are related to the difference between their transport gaps (see Figs. S5–S7 of the ESI†).

Additionally, the CIS-calculation performed for the free CBZ and TBZ molecules, by which we are able to unveil the origin and final states contributing to transitions giving rise to particular excitation, and their corresponding % weights and oscillator strengths can be used to estimate the efficiency of the first dipole-allowed excitation in both free molecules by a direct comparison of their associated oscillator strengths. The dimensionless oscillator strength values (expressing the probability for an excitation to produce) result in around 0.2 and 0.6 for the CBZ and TBZ free molecules, respectively, for their first HOMO → LUMO excitation (activating the fluorescence process after its decay). This result excellently agrees with the experimental fluorescence intensity observed for the CBZ and TBZ molecules in solution as shown in Fig. 2(A and D) where higher CBZ concentration is required to obtain a comparable fluorescence response (2.5 μM CBZ with respect to 100 nM TBZ).

To further study the mechanism leading to the decrease/increase of the fluorescence signal for the CBZ/TBZ molecules, respectively, before and after interaction with MoS_2, we have studied the morphology and spatial distribution of the HOMO and LUMO molecular orbitals, responsible for the most important transition in fluorescence emission.

Fig. 4 shows the computed iso-surfaces for the HOMO and LUMO molecular orbitals for CBZ and TBZ in both free and deposited on MoS_2 forms. These orbitals are those that contribute the most to the florescence mechanism, as explained above. Although a rationalization purely based on HOMO/LUMO distribution has to be carried out with caution, important knowledge can be acquired by a simple inspection of the molecular orbital spatial distribution. In the case of the free CBZ molecule (see Fig. 4A) both orbitals are mostly located in the fluorescent benzimidazole group ($C_7H_6N_2$), which makes

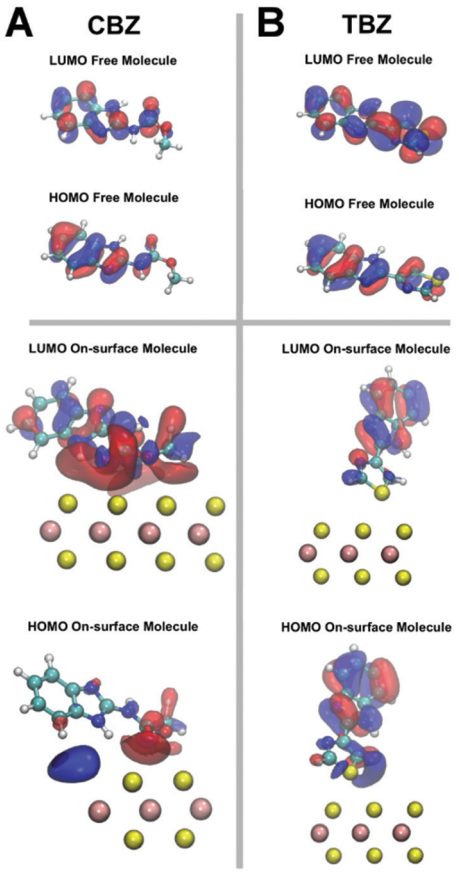

Fig. 4 Computed iso-surfaces at 0.05 $e^{-}Å^{-3}$ of molecular orbitals for: (a) HOMO and LUMO of free CBZ, and molecular HOMO and LUMO of CBZ on MoS_2, and (b) HOMO and LUMO of free TBZ, and molecular HOMO and LUMO of TBZ on MoS_2. Red and blue iso-surfaces correspond to positive and negative regions of the wave functions, respectively.

the transition between both states efficient, in agreement with the experimental observation. Nonetheless, when the CBZ molecule is adsorbed on the MoS_2 substrate, the system tends to restructure the LUMO spatial location from the benzimidazole group towards the non-fluorescent molecular group (see Fig. 4A), which hinders the efficiency of the fluorescence mechanism, as evidenced by the experiments.

For the case of the free TBZ (see Fig. 4B), also both HOMO and LUMO are located in the benzimidazole group making the fluorescence of the free molecule efficient. This scenario is maintained when the TBZ molecule is adsorbed on the MoS_2 substrate. In this case, the molecule/substrate interaction is mainly driven by a mixture of a sort of substrate/adsorbate Pauli repulsion with electrostatic anchoring, being able to slightly disrupt the adsorbed molecular geometry to redistribute the molecular LUMO from the thiazole group toward the fluorescent group (Fig. 4B), which dramatically improves the efficiency of the fluorescence, just as observed in the experiment. Importantly in this case, there is a charge rearrangement and orbital deformation, which favours fluorescence,

and it is neither caused by a charge transfer nor by chemical bonds, given the weak non-covalent nature of the interfacial interaction, but has the effect to reduce the overlap of the surface charge density of MoS_2 with the charge density of the adsorbate. We have checked that this LUMO on-surface restructuration vanishes for very large adsorption distances. Different types of deformation and restructuration of molecular orbitals by external perturbations, in particular by weak and electrostatic interactions with surfaces and other molecules as in the present case, have been extensively reported in previous literature.[28–30]

Interestingly, our results are fully compatible with a surface-mediated AIE process, in which the intramolecular rotation of the aromatic subunits of the TBZ is restricted upon non-covalent surface adsorption. On this basis, TBZ could *a priori* dissipate energy in a nonradiative form by the intramolecular relative rotation of its aromatic subunits. Nonetheless, this intramolecular rotation in TBZ seems to be hindered by an increase in the rigidity of the C–C bond linking the subgroups by effect of the interaction with the MoS_2 surface. Therefore, the nonradiative decay by molecular motion between the thiazole and benzimidazole groups in TBZ is inhibited, enhancing in this way the radiative decay and so the fluorescence signal. This rationalization allows us to easily explain why fluorescence enhancement in the presence of MoS_2 2D nanosheets is only detected for the TBZ, whilst for other similar fluorescent molecules such as CBZ, BN and quinine the emission properties are quenched by the light-harvesting material. To confirm this surface-mediated AIE, we have carried out a series of DFT calculations for TBZ in its free and on-surface adsorbed forms to estimate the stiffness of the linking C–C bond against the intramolecular rotation of the TBZ aromatic subunits. Calculations consist of computing the total energy of the TBZ molecule at different steps in a rigid rotation between its two aromatic subunits in a range between −30° and 30°. Calculations reveal that a rigidization of the bond of around one order of magnitude occurs from the free form to be adsorbed on the MoS_2 surface (see section S5 and Fig. S8 of the ESI†), which is consistent with the hypothesis. Thus, our observed fluorescence enhancement is directly related to a surface-mediated AIE,[17] where the nonradiative dissipation energy is inhibited by the rigidization of molecular rotational degrees of freedom after the molecular aggregation.[18]

A highly specific and sensitive method for TBZ sensing

Analytical data

Calibration. From the experiments shown in Fig. 1, we can conclude that, although TBZ exhibits an increase of its native fluorescence as a consequence of its interaction with all the TMDs prepared, the highest signal increase is obtained working with WS_2 (90 nm) exfoliated in EtOH/H_2O. Therefore, this system was selected to test the analytical performance of these nanomaterials towards TBZ determination. To this end, different WS_2 amounts were evaluated for the construction of calibration curves. The results, shown in Fig. 5, show that a linear increase in the fluorescence signal is produced because of the increase of TBZ concentration, irrespective of the amount of TMD employed. The use of 50 μL of WS_2 leads to the lowest sensitivity. Note that 100 μL of TMD suspension is enough to ensure the interaction with TBZ, leading to the maximum analytical signal for each assayed fungicide concentration in the linear range. Therefore, if a higher WS_2 amount is used (200 μL), no difference in the calibration plot is recorded.

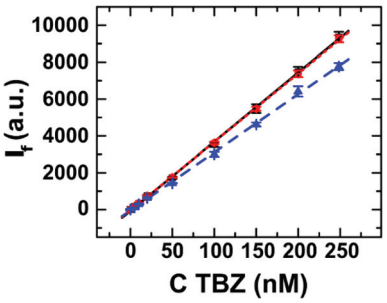

Fig. 5 Calibration curves of TBZ with 200 μL (black squares, solid line), 100 μL (red circles, dotted line) and 50 μL (blue triangles, dashed line) of WS_2 90 nm, 7.5 mg mL^{-1} in EtOH : H_2O (45 : 55, v/v). λ_{exc} = 294 nm; λ_{em} = 350 nm.

From the calibration curves recorded for 100 μL of WS_2, the fluorescence signal increases linearly with TBZ concentration according to $I_F = (37.1 \pm 0.8) \times 10^3$ C (μM) + (29 ± 1) with an agreement factor of 0.9996 in the 5–250 nM range. The proposed methodology allows TBZ analysis at the nM level showing a detection limit ($3\sigma_b$/slope) of 2.7 nM. This detection limit is similar to or even better than others previously reported for TBZ determination using either luminescence techniques including room-temperature phosphorescence (RTP), electrochemical methods or more sophisticated procedures such as liquid chromatography and capillary electrophoresis (see Table S1 [22,23,39–47] in the ESI†).

In addition, we have measured the accuracy and reproducibility of the proposed methodology evaluating the relative error (E_r, %) and the relative standard deviation (RSD, %) values at different concentration levels within the linear range. From these results, E_r values lower than 6.1% and RSD (%, n = 5) in the 1.1–4.1 range reveal that the method presents adequate accuracy and reproducibility.

Selectivity assays. In order to test the selectivity of the method, different pesticides (CBZ, BN and DI, diuron) were assayed as potential interfering compounds in the TBZ determination. To this end, increasing interfering amounts were added to a 20.0 nM TBZ solution containing 100 μL of WS_2 before the fluorescence was recorded. It was considered that interference occurs at a concentration level that produced a change of 10% in the initial TBZ signal. The results showed that none of the three pesticides produced interference in the TBZ determination up to concentrations of 500 nM, for CBZ and BN, and of 1.00 μM in the case of DI, which represents 25 and 50 fold the amount of TBZ in solution. As stated above,

Table 1 Recovery and relative standard deviation, RSD(%), values for TBZ determination in river samples

TBZ added [nM]	TBZ found [nM]	$RSD_{(n=3)}$ [%]	Recovery [%]
9.94	10.2	1.5	103
20.0	22.0	6.0	110
40.0	37.1	5.0	93

the presence of the S atom in the TBZ structure leads to a particular interaction of this analyte with the TMD, which allows the development of a highly sensitive but also selective method for this fungicide analysis with respect to other similar pesticides.

Analytical application. River water samples were selected as real matrices to test the performance of the proposed methodology. As stated in the Experimental section, samples were analysed without any additional pre-treatment except filtration. Calibration curves employing river water samples and following the standard addition procedure were constructed. To this end, aliquots of 200 μL of river water were spiked at different TBZ concentration levels, mixed with 100 μL of WS_2 suspensions and diluted to a 5.00 mL final volume. An additional sample consisting of 200 μL of river water diluted to 5.00 mL was prepared. From the fluorescence data recorded from all these samples, a linear increase in the fluorescence intensity with a slope of (36.1 ± 1.6) nM^{-1} was obtained. This slope value is similar to that found by the external calibration in Fig. 5 (37.1 ± 0.8) nM^{-1}, which was obtained measuring the fluorescence of solutions containing increasing TBZ concentrations without river water. These results could allow us to conclude that none of the compounds presented in the real sample disturbs the analytical signal recorded. To confirm this statement, we applied the Student's *t*-test to compare statistically these slopes. We obtain $t_{exp} = 0.99$, a value which is lower than the tabulated one, $t_{tab} = 2.20$ (95%), indicating that there is no significant statistical difference in the slope values. Therefore, we can conclude that no matrix interference is produced and the quantification of TBZ in river samples can be performed by direct interpolation of the fluorescence signal in the calibration graph (Fig. 5). The assays, described in section 4.5, were carried out in triplicate and a summary of the results is shown in Table 1. As shown, the proposed methodology can be applied in these kinds of samples, with good reproducibility and excellent recovery values.

Experimental

Materials

Molybdenum(IV) sulphide powder of 2 μm and 90 nm particle diameter, tungsten(IV) sulphide (90 nm), thiabendazole (TBZ), quinine (Q) sulphate salt monohydrate, carbendazim (CBZ), diuron (DI) and benomyl (BN) all 99% were supplied by Sigma-Aldrich Chemical Co. (St Louis, USA). Sulphuric acid, 1-methyl-2-pyrrolidinone (NMP) and ethanol (EtOH) were provided by Scharlau (Barcelona, Spain). 1 mM TBZ standard solutions were prepared in ethanol. TBZ solutions were daily prepared from the stock by dilution in water. Ultrapure water was produced by a system of Merck Millipore (Billerica, Massachusetts, USA).

Apparatus

Fluorescence measurements were carried out with an F-7000 fluorescence spectrophotometer from Hitachi High-Technologies Co. (Tokyo, Japan) equipped with a 1.0 cm quartz cuvette. The solvent-assisted exfoliation of the TMDs was done with a Transonic 570/H ultrasonic bath supplied by Elma Schmidbauer GmbH (Singen, Germany). The subsequent step to obtain a TMD suspension was performed with a centrifuge Rotofix 32A purchased from Hettich GmbH & Co.KG (Tuttlingen, Germany).

Synthesis of 2D nanomaterials

The procedure followed for the synthesis of TMD suspensions was previously reported.[7] Briefly described: 75 mg of TMD (90 nm and 2 μm MoS_2 or 90 nm WS_2) were weighed in a glass vial and 10 mL of the dispersion solvent (NMP or EtOH/water, 45/55 v : v) were subsequently added. Once the vial was sealed, the mixture was subjected to batch ultrasonication for 2 h and the mixture was centrifuged at 1500 rpm for 45 minutes to remove aggregates. The supernatant was collected and kept at 4 °C until use. MnO_2 nanosheets were prepared according to the procedure described by Wu *et al.*[31] GOx was synthesized by a modified Hummers' method as described before.[32]

Fluorescence measurements

To investigate the effect of 2D nanomaterials on pesticide fluorescence, TBZ solutions were prepared by mixing, in a 5.00 mL volumetric flask, a volume of TBZ stock solution and a fixed amount of the nanomaterial suspension, before filling it to the graduation mark with water. Next, fluorescence spectra were recorded at an excitation wavelength of 294 nm and at room temperature. This procedure was also followed for the preparation and measurement of CBZ and BN but, in these cases, excitation was produced at 280 nm. Quinine solutions were prepared in 0.05 M sulphuric acid aqueous solution and the fluorescence was registered with a 346 nm excitation beam.

Analytical application

To test the performance of the method, water samples collected from Záncara River, located in the central area of Spain, were used as real samples in this study. The samples were filtered (through 0.45 μm) and stored at 4 °C until use. As TBZ was not detected in this river sample, different river water samples were initially spiked at three different TBZ concentration levels and subsequently analysed by external calibration to evaluate the recovery obtained using the developed methodology in these kinds of matrices. To this end, aliquots of 200 μL of spiked river water were mixed with 100 μL of WS_2 suspensions in $EtOH/H_2O$ (45/55, v/v) and diluted to 5.00 mL final volume before the fluorescence measurement.

Theoretical methods

All the static simulations have been performed by using density functional theory (DFT) as implemented in the QUANTUM ESPRESSO simulation package.[33] Exchange–correlation interactions have been accounted for by the generalized gradient approximation (GGA) within the Perdew–Burke–Ernzerhof (PBE) parametrization.[34] The Vanderbilt ultrasoft pseudopotential scheme[35] has been adopted to model the ion-electron interactions, and the DFT+D2 method has been used to account for dispersive forces to conventional DFT functionals.[36] A time-dependent DFT (TDDFT) formalism implemented in QUANTUM ESPRESSO[33] has been employed to compute the excitation spectra of all systems (see ref. 33 and references therein), and the GAUSSIAN09 package[37] to obtain oscillator strengths, and elucidate transitions and electronic states involved in the most intense excitation in the gas-phase molecules within the B3LYP/cc-pVTZ level of theory by means of the configuration interaction single-excitation (CIS) formalism[38] (an extended description of the computational details can be found in the ESI†).

Interfacial models

The periodic interfacial systems have been computed by relaxing a large set of different starting configurations with the two molecules in five different positions and orientations on each different substrate (see the ESI†). Before computing the complete interfaces the CBZ and TBZ molecules were optimized in their gas-phase form and afterwards used as starting-point geometries to be deposited on the single layers. The MoS_2 and graphene (Gr) substrate single layers analysed have been modelled by (6 × 3) and (8 × 4) periodicities, respectively, with only one molecule per unit cell. The graphene oxide (GOx) substrate has been modelled by attaching an OH group on top of graphene C atoms homogeneously with a (2 × 2) periodicity referred to the graphene sheet. The unit cell sizes adopted are enough to avoid undesirable intermolecular interactions arising between neighbouring cells, with a minimum perpendicular distance between them >20 Å.

Conclusions

In this work we have shown that the interaction of a TBZ molecule, a widespread used fungicide that may cause important diseases, with nanoplatforms of TMDs and particularly of WS_2, leads to a significant increase in the fluorescence yield. The mechanism leading to this enhancement has been rationalized by DFT calculations and found to be related to the molecular interaction and bonding rigidization after non-covalent adsorption of TBZ on the surface, in a kind of surface-mediated AIE process. The stiffness of the C–C bond connecting the aromatic subunits of the TBZ molecule once interacting with the MoS_2 nanosheets inhibits the nonradiative decay by molecular motion and enhances the fluorescence channel. We show that this unusual behavior is specific for TBZ on TMDs, and does not operate either for other molecules of the same benzimidazole family or for other 2D materials (graphene, graphene oxide).

We show that this unusual behaviour is specific for TBZ on TMDs, and does not operate either for other molecules of the same benzimidazole family or for other 2D materials (graphene, graphene oxide). This specificity has allowed us to develop a simple, robust, high-sensitive and selective method towards TBZ determination that can be applied to real river water samples with very good recovery and precision, avoiding indeed laborious, overpriced and time-consuming sample treatments. We foresee that this mechanism could be generalized to any other fluorescence molecules with stiff C–C bonds between the molecular subunits upon surface interaction that slightly redistributes their LUMO orbitals after non-covalent adsorption.

Conflicts of interest

There are no conflicts to declare.

Acknowledgements

The authors acknowledge financial support from the Spanish MINECO (MAT2017-85089-C2-1-R, MAT2017-85089-C2-2-R) and the EU *via* the ERC-Synergy Program (grant ERC-2013-SYG-610256 NANOCOSMOS) and Horizon 2020 Research and Innovation Program (Graphene Flagship-core2 – 785219) and the Comunidad Autónoma de Madrid (P2018/NMT-4349, TRANSNANOAVANSENS-CM and P2018/NMT-4367 FOTOART). J. I. M. acknowledges the support by the "Ramón y Cajal" Program of MINECO (grant RYC-2015-17730).

References

1 C. Tan, X. Cao, X.-J. Wu, Q. He, J. Yang, X. Zhang, J. Chen, W. Zhao, S. Han, G.-H. Nam, M. Sindoro and H. Zhang, *Chem. Rev.*, 2017, **117**, 6225–6331.
2 D. Jariwala, V. K. Sangwan, L. J. Lauhon, T. J. Marks and M. C. Hersam, *ACS Nano*, 2014, **8**, 1102–1120.
3 C. Li, Q. Cao, F. Wang, Y. Xiao, Y. Li, J.-J. Delaunay and H. Zhu, *Chem. Soc. Rev.*, 2018, **47**, 4981–5037.
4 K. F. Mak and J. Shan, *Nat. Photonics*, 2016, **10**, 216–226.
5 H. Y. Song, Y. N. Ni and S. Kokot, *Biosens. Bioelectron.*, 2014, **56**, 137–143.
6 D. Zhu, W. Liu, D. X. Zhao, Q. Hao, J. Li, J. X. Huang, J. Y. Shi, J. Chao, S. Su and L. H. Wang, *ACS Appl. Mater. Interfaces*, 2017, **9**, 35597–35603.
7 M. D. Petit-Dominguez, C. Quintana, L. Vazquez, M. del Pozo, I. Cuadrado, A. M. Parra-Alfambra and E. Casero, *Microchim. Acta*, 2018, **185**, 334.
8 A. M. Parra-Alfambra, E. Casero, L. Vazquez, C. Quintana, M. del Pozo and M. D. Petit-Dominguez, *Sens. Actuators, B*, 2018, **274**, 310–317.

9 Y. Wang, J. Hu, Q. Zhuang and Y. Ni, *ACS Sustainable Chem. Eng.*, 2016, **4**, 2535–2541.
10 Kenry, A. Geldert, Z. Lai, Y. Huang, P. Yu, C. Tan, Z. Liu, H. Zhang and C. T. Lim, *Small*, 2017, **13**, 1601925.
11 X. Liu, W. Zhang, L. Huang, N. Hu, W. Liu, Y. Liu, S. Li, C. Yang, Y. Suo and J. Wang, *Microchim. Acta*, 2018, **185**, 234–234.
12 S. C. Chen, C. Y. Lin, T. L. Cheng and W. L. Tseng, *Adv. Funct. Mater.*, 2017, **27**, 1702452.
13 S. Gogoi and R. Khan, *Phys. Chem. Chem. Phys.*, 2018, **20**, 16501–16509.
14 D.-K. Ji, Y. Zhang, Y. Zang, J. Li, G.-R. Chen, X.-P. He and H. Tian, *Adv. Mater.*, 2016, **28**, 9356–9363.
15 Y.-H. Ma, W.-T. Dou, Y.-F. Pan, L.-W. Dong, Y.-X. Tan, X.-P. He, H. Tian and H.-Y. Wang, *Adv. Mater.*, 2017, **29**, 1604253.
16 J.-X. Song, X.-Y. Tang, D.-M. Zhou, W. Zhang, T. D. James, X.-P. He and H. Tian, *Mater. Horiz.*, 2017, **4**, 431–436.
17 J. Chen, B. Xu, X. Ouyang, B. Z. Tang and Y. Cao, *J. Phys. Chem. A*, 2004, **108**, 7522–7526.
18 Z. He, C. Ke and B. Z. Tang, *ACS Omega*, 2018, **3**, 3267–3277.
19 R. Romero-Cano, D. Kassuha, J. Peris-Vicente, P. Roca-Genoves, S. Carda-Broch and J. Esteve-Romero, *Analyst*, 2015, **140**, 1739–1746.
20 G. R. da Silva, J. A. Lima, L. F. de Souza, F. A. Santos, M. A. G. Lana, D. C. S. de Assis and S. d. V. Cancado, *Talanta*, 2017, **171**, 307–320.
21 J. Jiang, S. Zou, L. Ma, S. Wang, J. Liao and Z. Zhang, *ACS Appl. Mater. Interfaces*, 2018, **10**, 9129–9135.
22 M. Kaur, P. Raj, N. Singh, A. Kuwar and N. Kaur, *ACS Sustainable Chem. Eng.*, 2018, **6**, 3723–3732.
23 Y. Dong, L. Yang and L. Zhang, *J. Agric. Food Chem.*, 2017, **65**, 727–736.
24 C. Lu, Y. Liu, Y. Ying and J. Liu, *Langmuir*, 2017, **33**, 630–637.
25 J. Conesa-Egea, J. Gallardo-Martinez, S. Delgado, J. I. Martinez, J. Gonzalez-Platas, V. Fernandez-Moreira, U. R. Rodriguez-Mendoza, P. Ocon, F. Zamora and P. Amo-Ochoa, *Small*, 2017, **13**, 1700965.
26 J. Conesa-Egea, N. Nogal, J. I. Martinez, V. Fernandez-Moreira, U. R. Rodriguez-Mendoza, J. Gonzalez-Platas, C. J. Gomez-Garcia, S. Delgado, F. Zamora and P. Amo-Ochoa, *Chem. Sci.*, 2018, **9**, 8000–8010.
27 J. Troyano, O. Castillo, J. I. Martinez, V. Fernandez-Moreira, Y. Ballesteros, D. Maspoch, F. Zamora and S. Delgado, *Adv. Funct. Mater.*, 2018, **28**, 1704040.
28 C. Tang, W. Guo and Y. Guo, *Appl. Phys. Lett.*, 2006, **88**, 243112.
29 P. Hapala, M. Svec, O. Stetsovych, N. J. van der Heijden, M. Ondracek, J. van der Lit, P. Mutombo, I. Swart and P. Jelinek, *Nat. Commun.*, 2016, **7**, 11560.
30 J. Li and R.-Q. Zhang, *Sci. Rep.*, 2016, **6**, 22304.
31 S. Wu, C. Chen, H. Yang, W. Wei, M. Wei, Y. Zhang and S. Liu, *Sens. Actuators, B*, 2018, **273**, 1047–1053.
32 E. Casero, A. M. Parra-Alfambra, M. D. Petit-Dominguez, F. Pariente, E. Lorenzo and C. Alonso, *Electrochem. Commun.*, 2012, **20**, 63–66.
33 P. Giannozzi, S. Baroni, N. Bonini, M. Calandra, R. Car, C. Cavazzoni, D. Ceresoli, G. L. Chiarotti, M. Cococcioni, I. Dabo, A. Dal Corso, S. de Gironcoli, S. Fabris, G. Fratesi, R. Gebauer, U. Gerstmann, C. Gougoussis, A. Kokalj, M. Lazzeri, L. Martin-Samos, N. Marzari, F. Mauri, R. Mazzarello, S. Paolini, A. Pasquarello, L. Paulatto, C. Sbraccia, S. Scandolo, G. Sclauzero, A. P. Seitsonen, A. Smogunov, P. Umari and R. M. Wentzcovitch, *J. Phys.: Condens. Matter*, 2009, **21**, 395502.
34 J. P. Perdew, K. Burke and M. Ernzerhof, *Phys. Rev. Lett.*, 1996, **77**, 3865–3868.
35 D. Vanderbilt, *Phys. Rev. B: Condens. Matter Mater. Phys.*, 1990, **41**, 7892–7895.
36 S. Grimme, *J. Comput. Chem.*, 2006, **27**, 1787–1799.
37 M. J. Frisch, G. W. Trucks, H. B. Schlegel, G. E. Scuseria, M. A. Robb, J. R. Cheeseman, G. Scalmani, V. Barone, G. A. Petersson, H. Nakatsuji, X. Li, M. Caricato, A. Marenich, J. Bloino, B. G. Janesko, R. Gomperts, B. Mennucci, H. P. Hratchian, J. V. Ortiz, A. F. Izmaylov, J. L. Sonnenberg, D. Williams-Young, F. Ding, F. Lipparini, F. Egidi, J. Goings, B. Peng, A. Petrone, T. Henderson, D. Ranasinghe, V. G. Zakrzewski, J. Gao, N. Rega, G. Zheng, W. Liang, M. Hada, M. Ehara, K. Toyota, R. Fukuda, J. Hasegawa, M. Ishida, T. Nakajima, Y. Honda, O. Kitao, H. Nakai, T. Vreven, K. Throssell, J. A. Montgomery Jr., J. E. Peralta, F. Ogliaro, M. Bearpark, J. J. Heyd, E. Brothers, K. N. Kudin, V. N. Staroverov, T. Keith, R. Kobayashi, J. Normand, K. Raghavachari, A. Rendell, J. C. Burant, S. S. Iyengar, J. Tomasi, M. Cossi, J. M. Millam, M. Klene, C. Adamo, R. Cammi, J. W. Ochterski, R. L. Martin, K. Morokuma, O. Farkas, J. B. Foresman and D. J. Fox, *Gaussian 09, Revision E.01*, Gaussian, Inc., Wallingford, CT, 2016.
38 J. B. Foresman, M. Headgordon, J. A. Pople and M. J. Frisch, *J. Phys. Chem.*, 1992, **96**, 135–149.
39 E. S. Sousa, L. Pinto and M. C. U. de Araujo, *Microchem. J.*, 2017, **134**, 131–139.
40 J. Peris-Vicente, P. Roca-Genoves, K. Tayeb-Cherif and J. Esteve-Romero, *Electrophoresis*, 2016, **37**, 2517–2521.
41 A. Segura-Carretero, C. Cruces-Blanco, B. Canabate-Diaz, J. F. Fernandez-Sanchez and A. Fernandez-Gutierrez, *Anal. Chim. Acta*, 2000, **417**, 19–30.
42 B. Tang, X. Wang, G. L. Wang, Y. Wang and Z. Z. Chen, *Analyst*, 2005, **130**, 1038–1045.
43 S. Takeda, K. Fukushi, K. Chayama, Y. Nakayama, Y. Tanaka and S. Wakida, *J. Chromatogr. A*, 2004, **1051**, 297–301.
44 A. M. Oliveira, H. C. Loureiro, F. F. S. de Jesus and D. P. de Jesus, *J. Sep. Sci.*, 2017, **40**, 1532–1539.
45 X. D. Zhong, D. S. Fu, P. P. Wu, Q. Liu, G. C. Lin, S. H. Cao and Y. Q. Li, *Anal. Methods*, 2014, **6**, 7260–7267.
46 Q. Tang, J. Zhang, T. Sun, C. H. Wang, Y. Huang, Q. D. Zhou and G. Wei, *Spectrochim. Acta, Part A*, 2018, **191**, 372–376.
47 M. Asghar, M. Yaqoob, N. Munawar and A. Nabi, *Anal. Sci.*, 2016, **32**, 337–342.

